CHINESE JOURNAL OF PHYSICS VOL. 52, NO. 1-I February 2014

The Microstructure of Pbte-Bi_2Te_3 Alloys and Their Thermoelectric Properties

HeeJin Kim,[1,2] Ji-eun Park,[1] Mi-Kyung Han,[1,*] Sung-Jin Kim,[1,†] and Wooyoung Lee[2,‡]

[1]*Department of Chemistry and Nano Sciences, Ewha Womans University, 120-750 Seoul, Korea*

[2]*Department of Materials Science and Engineering, Yonsei University, 120-749 Seoul, Korea*

(Received January 2, 2013)

The $(PbTe)_x$-$(Bi_2Te_3)_{100-x}$ alloy (x = 0, 3, 5, 7) samples were prepared by adding PbTe nanoparticles into a bulk Bi_2Te_3 matrix using typical solid state synthetic reactions. PbTe-Bi_2Te_3 alloy samples were studied by powder X-ray diffraction (PXRD), selected area electron diffraction (SAED), convergent beam electron diffraction (CBED), and energy dispersive spectroscopy (EDS). The results of the microstructural analysis showed that the PbTe-Bi_2Te_3 system contains three types of phase, a Bi_2Te_3 phase, a $Pb_xBi_{2-x}Te_3$ solid solution, and a $PbBi_2Te_4$ phase depending on the PbTe concentration. The $Pb_xBi_{2-x}Te_3$ solid solution in the Bi_2Te_3 matrix scatters not in electrons but phonons, thereby reducing the thermal conductivity. On the other hands, the $PbBi_2Te_4$ phase in the Bi_2Te_3 matrix scatters not only phonons but also electrons. As a result, the maximum values of 0.6 were obtained for the dimensionless figure of merit ZT for the $(PbTe)_3$-$(Bi_2Te_3)_{97}$ alloy at room temperature values of 0.6 are obtained for the $(PbTe)_3$-$(Bi_2Te_3)_{97}$ alloy at room temperature.

DOI: PACS numbers:

I. INTRODUCTION

Thermoelectric materials which can interconvert thermal into electrical energy have been applied in many fields such as refrigeration and power generation [1–3]. The performance of a thermoelectric material can be evaluated in terms of a dimensionless figure of merit, ZT, defined as $(S^2\sigma/\kappa)T$, where S is the Seebeck coefficient, σ the electrical conductivity, κ the thermal conductivity, and T the temperature in Kelvin. A high ZT value can be obtained by a high power factor ($S^2\sigma$) and a low thermal conductivity. However, the Seebeck coefficient, electrical conductivity, and thermal conductivity are dependent on the carrier concentration and mobility, which is impossible to control independently. In a thermoelectric material with nanostructures, improved ZT is expected due to quantum confinement and reduction of thermal conductivity [4–6]. Recently, thermoelectric materials with nanostructure have been reported to have much higher ZT values than bulk materials due to decreasing of the thermal conductivity [7–10]. Examples are the cesium intercalated

*Electronic address: mikihan@ewha.ac.kr
†Electronic address: sjkim@ewha.ac.kr
‡Electronic address: wooyoung@yonsei.ac.kr

bismuth telluride ($CsBi_4Te_6$), which measured a high ZT at low temperature [11], and the p-type Bi_2Te_3/Sb_2Te_3 superlattice thin film ZT=2.4 at room temperature by Venkatasubramanian *et al.* [5]. The p-Type $Bi_{0.52}Sb_{1.48}Te_3$ bulk material with low-dimensional structure was also reported as having a ZT of 1.5 at room temperature [12]. Most of these studies were focused on the lower thermal conductivity, especially contributions by the phonons. Effective reduction of the thermal conductivity should be by scattered phonons without significantly interrupting the electrical conductivity. Therefore, an appropriate combination of matrix material and 2nd phase material in nanocomposites is expected to be important to achieve a high ZT [13].

Recent reports in a variety of journals have described the $A^{IV}B^{VI}$-$A_2^VB_3^{VI}$ (A^{IV} = Ge, Sn, Pb; A^V = Bi, Sb; B^{VI} =Se, Te) compounds as thermoelectric materials with multi-component systems [14–18], such as a GeTe-Bi_2Te_3 and GeTe-Sb_2Te_3 pseudobinary system [14], a PbTe-Sb_2Te_3 system [15], and a PbTe-Bi_2Te_3 system [16–18]. In the PbTe-Bi_2Te_3 system, Oosawa *et al.* [16] found that $PbBi_4Te_7$ possesses advantageous thermoelectric properties, and Yim *et al.* have reported that the highest Seebeck coefficient was -76 uV/K due to the $PbBi_4Te_7$ phase, the lowest resistivity value obtained was 4.81×10^{-4} Ω cm due the $PbBi_2Te_4$ phase, and the lowest thermal conductivity was 1.1 W/mK due to the existence of the metastable ternary phase and the phase separation [17]. Unfortunately, PbTe-Bi_2Te_3 compounds of the above journal reports exhibit relatively high thermal conductivity, because the structure of these samples are not a nanostructure, and for these compounds there does not occur the great reduction of the thermal conductivity due to not enough scattering of the phonons with the interfaces.

In this paper, we discussed the microstructure and thermoelectric properties of PbTe-Bi_2Te_3 alloys. Bi_2Te_3 and its alloys are the best thermoelectric materials available near room temperature with the highest ZT [19, 20]. And PbTe is one of the best thermoelectric materials used for thermoelectric generators in the temperature range 400–800 K over the last four decades [21]. We synthesize $(PbTe)_x$-$(Bi_2Te_3)_{100-x}$ alloy (x = 0, 3,5,7) samples by adding the PbTe nanoparticles in the standard solid state synthesis of Bi_2Te_3. We investigate the microstructure of the PbTe-Bi_2Te_3 alloys using powder X-ray diffraction (PXRD), selected area electron diffraction (SAED), convergent beam electron diffraction (CBED), and energy dispersive spectrometry (EDS), and report the effects of the PbTe nanoparticles on the thermoelectric properties of the PbTe-Bi_2Te_3 alloy. The Seebeck coefficients, electrical conductivities, and thermal conductivities were measured and compared with those of a Bi_2Te_3 ingot sample.

II. EXPERIMENT DETAILS

For the synthesis of the PbTe nanoparticles, Te-TOP solution (0.5 M for Te) was prepared by tellurium shot (99.999%, Aldrich) into trioctylphosphine (TOP, 90%, Aldrich) in a glovebox and a yellow solution was obtained. The mixture was heated to 423 K under an Ar atmosphere. Lead acetate trihydrate ($PbAc_2 \cdot 3H_2O$, 99.99+%, Aldrich), oleic acid (90%, Aldrich), and phenyl ether were mixed and heated to 473 K for 20 min under an

argon atmosphere. After the solution was cooled to 313 K, it was transferred into a glovebox and mixed with the Te-TOP solution in a bath. The reaction solution changed color from yellow to black immediately after the injection of the Te-TOP solution. After the reaction, the solution was cooled to room temperature and then centrifuged at 13,000 rpm for 30 min. The dark product was washed with acetone and dried in air at room temperature.

To synthesize the $(PbTe)_x$-$(Bi_2Te_3)_{100-x}$ alloy (x = 0,1,3,5,7) samples, stoichiometric amounts of elemental Bi (99.999%) and Te (99.999%) for Bi_2Te_3, and a specified amount of PbTe nanoparticles in weight percentage were loaded into silica tubes (10 mm diameter, 1 mm wall thickness) and then sealed under vacuum. The sealed tubes were heated to 1273 K over a period of 12 h, held there for 12 h, slowly cooled to 673 K over a period of 12 h, and finally quenched to room temperature. A series of samples consisting of 3, 5, and 7 wt% PbTe nanoparticles in the bulk Bi_2Te_3 matrix were prepared. In addition, the Bi_2Te_3 sample without nanoparticles was prepared under identical conditions to serve as a reference.

PXRD patterns were obtained with a Rigaku X-ray Diffractometer using Cu-K radiation (λ = 1.5418 Å) at 30 mA and 40 kV. The diffraction data were recorded at a scanning rate of 0.1° min^{-1}. The sample morphologies, fine structures, SAED, and CBED patterns were obtained by high-resolution transmission electron microscopy (HR-TEM; JEOL 2100F). EDS (Oxford, INCAx-sight) with a beam size of 0.2 nm diameter were used. Thin specimens for TEM were prepared using a precision ion polishing system (Gatan; Model 691).

The thermal conductivity was determined by using the thermal diffusivity, $\kappa = D \cdot C_p \cdot \rho$, where ρ, D, and C_p are the sample density, thermal diffusivity, and specific heat, respectively, of the sample. The sample density was measured by the Archimedes method and ranged from 7.2 to 7.6 g cm^{-1} at room temperature. The thermal diffusivity and specific heat were measured on Netzsch LFA-457 and DSC-404 instruments, respectively. To measure the thermal diffusivity, the samples were cut into disks with a diameter of about 10 mm and thickness of about 2 mm. For the measurement of the electrical properties, the samples were cut into rectangular shapes with dimensions of about $3 \times 3 \times 10$ mm^3. The electrical conductivity and Seebeck coefficient were measured concurrently under a low-pressure helium atmosphere from room temperature to approximately 580 K using a ULVAC-RIKO ZEM-3 instrument. The Seebeck coefficients were measured three times with different temperature gradients between 10 and 30 °C at each temperature step.

III. RESULTS AND DISCUSSION

The synthesis of the PbTe nanoparticles was confirmed by PXRD. Fig. 1(a) shows the PXRD pattern of the PbTe nanoparticles, in which all of the peaks were indexed based on the cubic lattice of PbTe (JCPDS 02-1132) [22] with Fm3m (225) symmetry. No peaks for lead, tellerium, or other lead-tellerium compounds were observed in the PXRD pattern. The TEM images, shown in Fig. 1(b), reveal that the PbTe nanoparticles are cubic shape with an average size of about 15 nm. The Fast Fourier transforms (FFTs) of the TEM

image (upper right in Fig. 1(b)) indicate that the particles are well crystallized with a face centered cubic symmetry. The FFT in Fig. 1(b) is oriented with its [110] zone axis perpendicular to the sample, and as a result the {200} and {111} reflections appear in the FFTs. The cell parameter of the a-axis calculated from the FFTs was 6.4 Å, which was close to the unit cell parameter calculated from the PXRD pattern. The synthesized binary PbTe nanoparticles were used as the inclusions for PbTe-Bi_2Te_3 alloy. In this synthetic condition, we presumed that PbTe was melted and re-crystallized, because its melting point (1197K) is lower than our synthetic temperature (1273 K). The PbTe-Bi_2Te_3 alloy samples were characterized by PXRD. All of the reflections in the PXRD pattern in Fig. 2(a) can be readily indexed as the rhombohedral lattice of Bi_2Te_3 (space group: $R\bar{3}m(166)$, JCPDS, No. 15-0863) [22], except for two satellite peaks at $2\theta = 19°$ and 49° of the 5 and 7wt% PbTe samples. In the pseudo-binary PbTe-Bi_2Te_3 system, $nPbTe{\cdot}mBi_2Te_3$ compounds (n = 1, 2 and m = 1–4) have been reported, such as $PbBi_8Te_{13}$ [23], $PbBi_6Te_{10}$ [23], $PbBi_4Te_7$ [24, 25], $Pb_2Bi_6Te_{11}$ [23, 26], and $PbBi_2Te_4$ [27]. Two weak diffraction peaks at $2\theta = 19°$ and 49° were indexed by comparing $nPbTe{\cdot}mBi_2Te_3$ compounds, resulting from the (009) and (027) peak of $PbBi_2Te_4$ (space group: $R\bar{3}m(166)$, JCPDS, No. 38-1232) [22]. PXRD patterns for 0, 3, 5, and 7 wt% PbTe samples were refined using the Rietveld method. Fig. 2(b) shows the a and c axis lattice parameters of the 0, 3, 5, and 7 wt% PbTe obtained in the analysis. The above results indicated that the a and c axis lattice parameters increased significantly at the 3 wt% PbTe sample. At the 5 and 7 wt% PbTe samples there was an increase gradually in the c axis lattice parameters, however the a axis lattice parameter remains almost unchanged. We suggest that the rapid increases of the a and c axis lattice parameters at 3 wt% PbTe sample reveal that the Pb^{2+} ions substitute for Bi^{3+}ions. The ionic radius of Pb^{2+} (0.119 nm) has a larger radius than that of Bi^{3+} (0.103 nm) [28]. Also, we suggest that the steady increases of the c axis lattice parameters and unvaried a axis lattice parameters at the 5 and 7 wt% PbTe samples were influenced by the $PbBi_2Te_4$ ternary phase (a = 0.4452 nm, c = 4.1531 nm). As a result, PbTe was melted and recrystallized in the synthetic process, partial Pb^{2+} ions substitute preferentially for Bi^{3+}ions to form $Pb_xBi_{2-x}Te_3$ solid solution, and the rest of the Bi^{3+} ions seem to format as the $PbBi_2$Te4 phase. From the above results, we found that the upper limit of the solubility of Pb in a Bi_2Te_3 matrix is close to 3 wt%. The $Pb_xBi_{2-x}Te_3$ solid solution and the formation of the $PbBi_2Te_4$ phase are provided by the TEM measurements. The HR-TEM image and SAED patterns of the 3 and 7 wt% PbTe samples are presented in Fig. 3 and 4, respectively. Fig. 3(a) shows a typical TEM image of the 3 wt% PbTe sample. TEM revealed that the grain size in the 3wt.% PbTe sample possessed average lengths of about 100–150 um. We tried to analyze by EDS these grains to find a $Pb_xBi_{2-x}Te_3$ solid solution, however Pb was not detected due to a very low Pb concentration. The CBED patterns taken from the Bi_2Te_3 matrix in the 0 and 3 wt% PbTe sample are shown in Fig. 3(b) and (c), respectively. Both the CBED and SAED patterns clearly reveal the rhombohedral structure. The CBED pattern can provide phase identification using primitive cell volume measurements. This method is known to be simple and accurate for the phase identification.

The primitive cell volume (Ω) of the real lattice can be calculated by the equation below.

$$\Omega = \frac{2 \cdot CL^4 \cdot \lambda^3}{D_1 \cdot D_2 \cdot \sin ANG \cdot (CRAD)^2};$$

where CL is the camera length, λ is the wavelength of the accelerating voltage in TEM, D_1 and D_2 are the distances of the Zero Order Laue Zone (ZOLZ) disks, ANG is the angle between the disks and $CRAD$ is the radius of the Higher Order Laue Zone (HOLZ) rings [29].

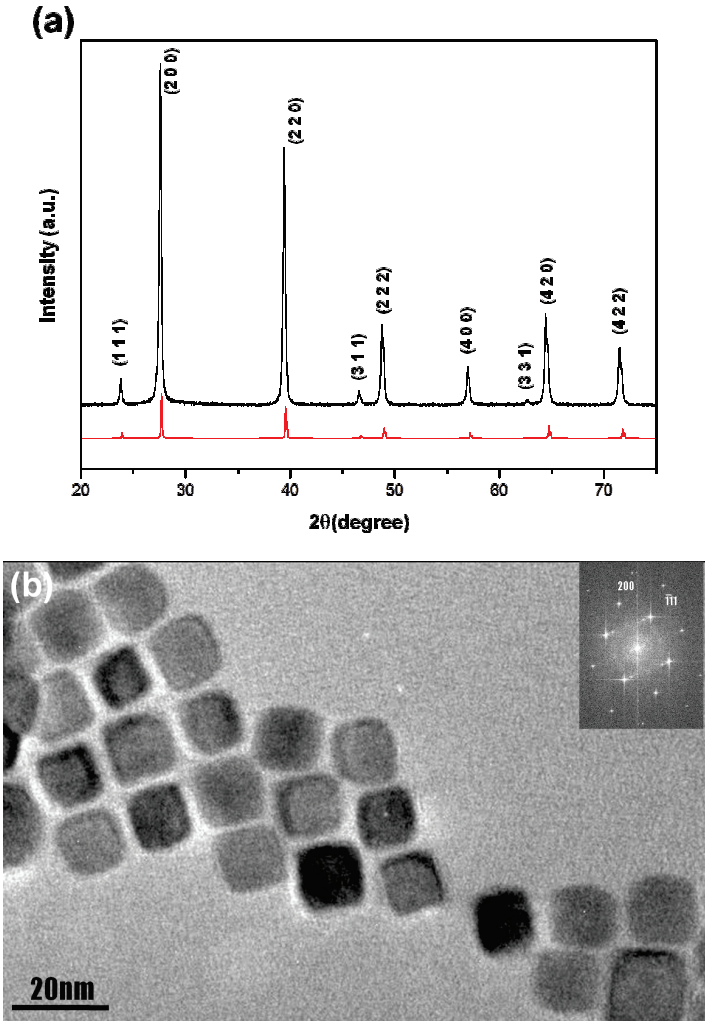

FIG. 1: (a) PXRD pattern of the PbTe nanoparticles, and (b) TEM and FFTs images of the synthesized PbTe nanoparticles.

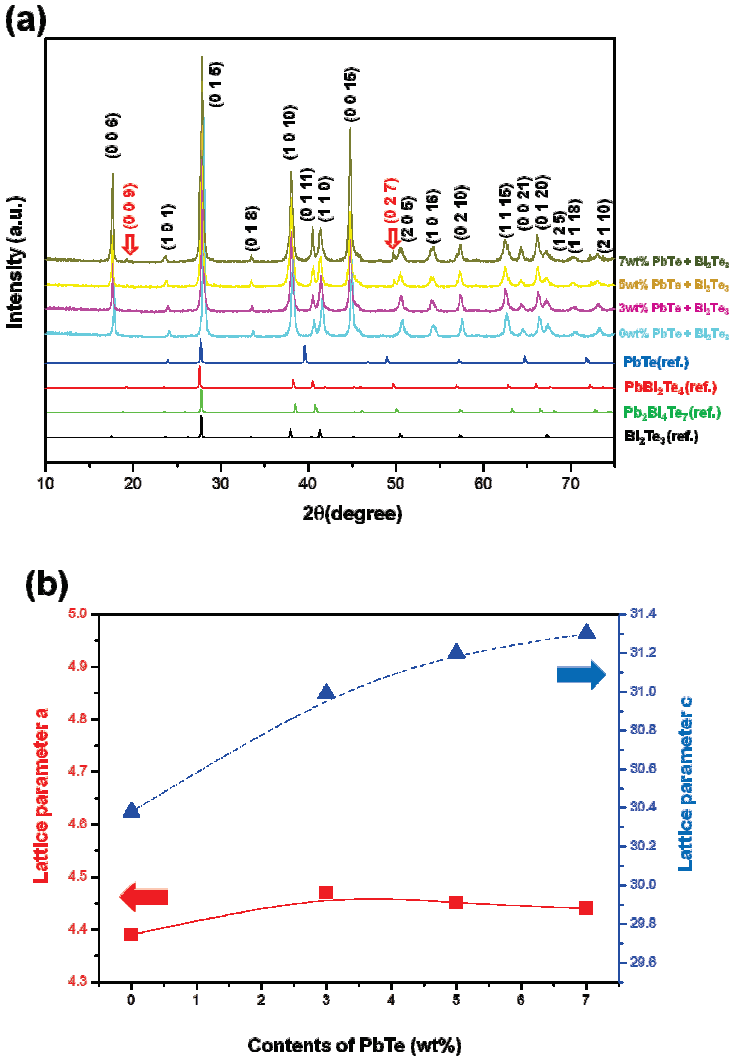

FIG. 2: (a) Powder XRD patterns of the PbTe-Bi_2Te_3 alloy samples compared with the XRD pattern of the related references. The arrow in the diffraction pattern indicates the diffraction from the $PbBi_2Te_4$ phase in the Bi_2Te_3 matrix. (b) Variation of the a and c axis lattice parameters depending on the PbTe contents.

The primitive cell volumes of 0 and 3 wt% PbTe sample were estimated to be about 504.55 Å^3 and 480.5 Å^3 from the CBED patterns, which are in a good agreement with the primitive cell volume obtained by the XRD values of the 0 and 3 wt% PbTe samples (507.04 Å^3, 479.56 Å^3). The CBED results indicate that the $PbxBi_{2-x}Te_3$ solid solution was formed in the 3 wt% PbTe sample. Fig. 4(a) shows a typical TEM image in the 7 wt% PbTe sample. The TEM image of the 7 wt% PbTe sample shows that the average grain

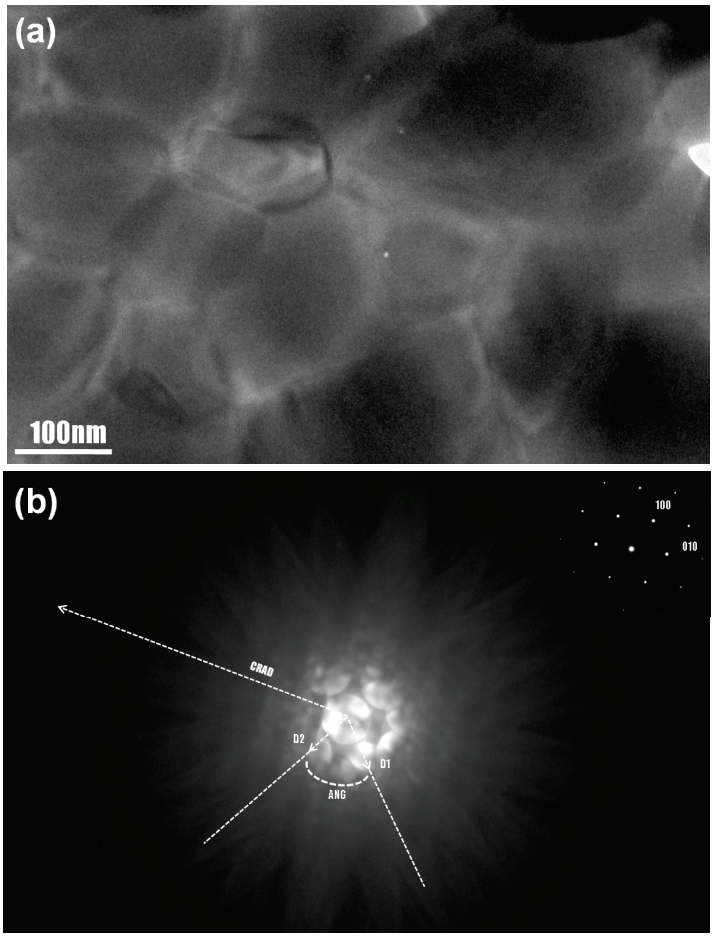

FIG. 3: (a) TEM image of the 3 wt% PbTe sample, (b) CBED pattern and SAED pattern (inset: upper right) of the 0 wt% PbTe sample, and (c) CBED pattern and SAED pattern (inset: upper right) of the 3 wt% PbTe sample.

size of this sample is smaller than that of the 3wt% PbTe sample, which is about 50–100 μm. Generally, the precipitations in the grain boundary prevent the grain growth due to the grain pinning effect. We paid attention to search for precipitations (10 $\sim$ 30 μm) in the grain boundary. (white arrows) HR-TEM image in the Fig. 4(b) shows that interfaces between the grain and the precipitation are incoherent or semicohernt. The microstructure with coherent interfaces could result in a significant lattice thermal conductivity reduction due to enhanced scattering of phonons by the difference in masses between the precipitates and the matrix [12] or bond stiffness [30]. However, incoherent or semicohernt interfaces reduced not only the lattice thermal conductivity but also the electric conductivity due to scattering both phonons and electrons. The EDS line profile analysis was carried out to investigate the composition of the precipitation. Fig. 4(c) shows the EDS line profile image of the Bi, Te, and Pb concentration in the precipitation region. As a result, we found that

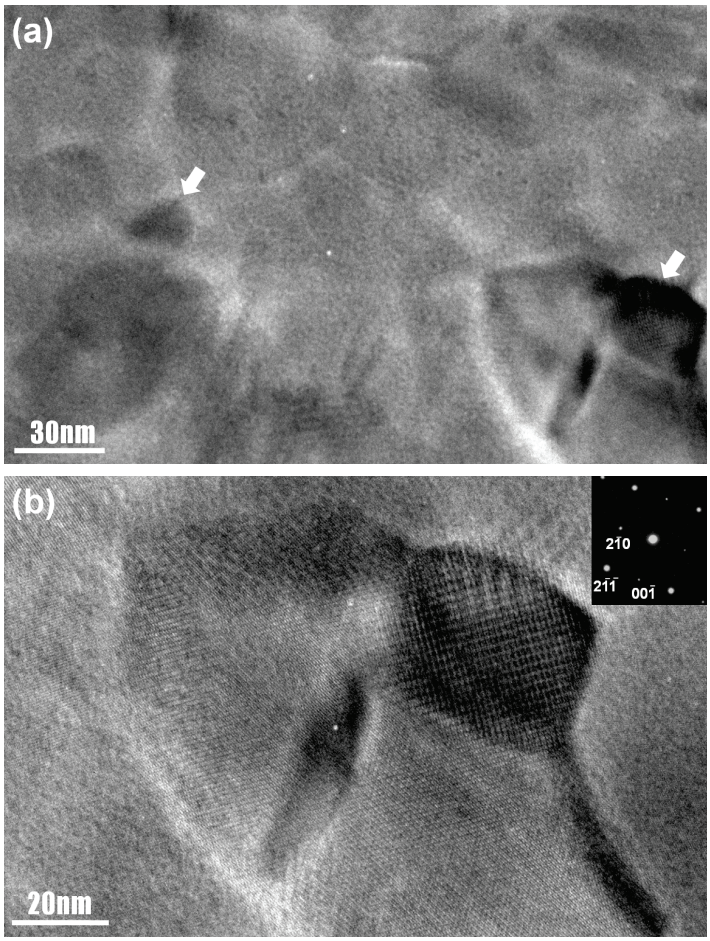

FIG. 4: (a) TEM image of the 7 wt% PbTe sample. The arrows in the TEM image indicate the precipitations from the $PbBi_2Te_4$ phase in the the Bi_2Te_3 matrix. (b) HR-TEM image of the interface between the precipitation and the matrix. (c) EDS line profile of the interface between the precipitation and the matrix.

the precipitation is the $PbBi_2Te_4$ phase. We suggest that the three types of phases are formed in the PbTe-Bi_2Te_3 system. One is matrix, which is composed of Bi_2Te_3, another is $Pb_xBi_{2-x}Te_3$ a solid solution phase, and the other is the $PbBi_2Te_4$ ternary phase. It is noticeable that the precipitations under 30 μm of $PbBi_2Te_4$ ternary phase are randomly dispersed in the grain boundary. These prevent the grain growth to keep the grain size. Finally, these phases influence the reduction of the lattice thermal conductivity.

Fig. 5 illustrates the dependence of the electronic transport properties on the concentration of PbTe in the PbTe-Bi_2Te_3 samples. All of the properties were measured in the same direction. The temperature dependence of the electrical conductivity, σ, is shown in Figure 5(a). In all cases, the electrical conductivity increases with increasing temperature over the measured temperature range and with decreasing PbTe content. The result for the

3 wt% PbTe sample shows a similar electrical conductivity (550 S/cm at room temperature) to the 0 wt% PbTe sample throughout the whole temperature ranges. This reveals that the $Pb_xBi_{2-x}Te_3$ solid solution phase did not influence significantly the electrical conductivity. The result for the 7 wt% PbTe sample shows an extremely low electrical conductivity (280 S/cm at room temperature). We suggest that this may be caused by the incoherent interfaces between the $PbBi_2Te_4$ and the Bi_2Te_3 matrix and the many grain boundaries induced by the $PbBi_2Te_4$ precipitations. We supposed that the incoherent or semicoherent interface between the matrix and the precipitation interrupted the electron transfer. Fig. 5(b) presents the temperature dependence of the Seebeck coefficient of the PbTe-Bi_2Te_3 samples. The Seebeck coefficient is negative in the whole temperature range, indicating that the majority of the charge carriers are electrons (n-type). As the temperature increases, the magnitude of the Seebeck coefficient of the samples decreases. The Seebeck coefficient for the 3 wt% PbTe sample ranges from -225 μV/K at room temperature to -128 μV/K at 580 K, whereas for the 7 wt% PbTe sample it ranged from ≈ -235 μV/K at room temperature to ≈ -160 μV/K at 580 K. The 7 wt% PbTe sample is higher than the other samples over the whole temperature range, which originates from an energy-filtering effect [31] due to the $PbBi_2Te_4$ preciptations. The electrical conductivity and Seebeck coefficient values were used to calculate the power factor, $S^2\sigma$, as shown in Figure 5(c). The 3 wt% PbTe sample shows a maximum power factor of 24.2 μW/cm $\cdot$ K^2 at room temperature due to the $Pb_xBi_{2-x}Te_3$ solid solution. The power factors of the samples with PbTe steadily decreases with increasing temperature, however the 0 wt% PbTe sample rapidly decreases with increasing temperature. The effects of these solid solution phase and ternary phase on the heat transport in these materials was studied with thermal diffusivity measurements as a function of temperature. Fig. 5(d) shows the temperature dependence of the total thermal conductivity of the 0, 3, 5, and 7 wt% PbTe samples. As expected, the total thermal conductivity decreases upon the addition of the PbTe nanoparticles. The total thermal conductivity, κ, consists of the phonon contribution, κ_{ph}, and the carrier contribution, κ_e, which is related to the electrical conductivity, σ, by the relation $\kappa_e = L_0\sigma T$, where L_0 is the Lorenz number ($L_0 = 1.53 \times 10^{-8}$ V^2 K^{-2}) [9]. The dashed line in Fig. 5(d) shows the phonon contribution to the total thermal conductivity. The κ_{ph} values of the 3, 5 wt%, and 7 wt% PbTe samples at room temperature are 0.94 W/m $\cdot$ K, 0.95 W/m $\cdot$ K, and 0.87 W/m $\cdot$ K, respectively. These values are smaller than that of the 0 wt% PbTe sample (κ_{ph} value $\approx$ 1.22 W/m $\cdot$ K at room temperature). It seems that the atomic disorder by the formation of $Pb_xBi_{2-x}Te_3$ solid solutions in the PbTe-Bi_2Te_3 system is essentially responsible for these low values. Furthermore, the noticeable reduction of the thermal conductivity observed in the 7 wt% PbTe sample seems to be due to the existence of incoherent interfaces in the $PbBi_2Te_4$ precipitations. It is clear from these results that the $Pb_xBi_{2-x}Te_3$ solid solutions and the $PbBi_2Te_4$ ternary phases in the PbTe-Bi_2Te_3 system cause a significant decrease in the lattice thermal conductivity. Fig. 6 shows the temperature dependencies of ZT for the 0, 3, 5 wt%, and 7 wt% PbTe samples. It can be seen that the ZT value decreases with increasing temperature. The highest ZT values were 0.6 in the 3 wt% PbTe sample at room temperature. The ZT of the 7 wt% PbTe sample was lower than that of the 0 wt% PbTe sample at room temperature, but higher at temperatures above 323 K, which is

mainly related to the thermal conductivity of the phonons. Also, this sample has a highest ZT value at 573 K. We supposed that the phonon contribution to the thermal conductivity was the important factor in the high temperature region. As a result, the $Pb_xBi_{2-x}Te_3$ solid solutions cause a significant decrease in the thermal conductivity without causing a significant reduction in the electrical conductivity. On the other hand, the incoherent boundaries induced in $PbBi_2Te_4$ precipitations cause a significant decrease not only in the thermal conductivity but also the electrical conductivity. Therefore, the formation of the solid solution and appropriate controlling of the precipitation are a highly effective way of enhancing the ZT values.

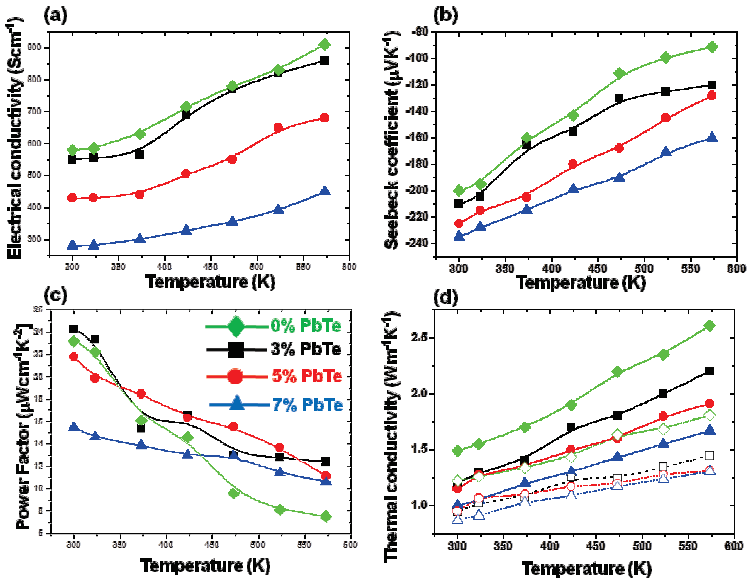

FIG. 5: Temperature dependence of (a) electrical conductivity, (b) Seebeck coefficient, (c) power factor, and (d) total thermal conductivity of the 0, 3, 5, and 7 wt% PbTe samples. The dashed line in Figure 5(d) indicates the phonon contribution to the thermal conductivity.

IV. CONCLUSIONS

The $(PbTe)_x$-$(Bi_2Te_3)_{100-x}$ alloy (x = 0,1,3,5,7) samples were prepared by PbTe nanoparticles into a bulk Bi_2Te_3 matrix. First, quadrilateral PbTe nanoparticles with a size about 15 nm were synthesized by combining lead acetate trihydrate with Te in trioctylphosphine (TOP) solution. PbTe-Bi_2Te_3 alloy samples were prepared by using typical solid state synthetic reactions with the Bi, Te elements and PbTe nanoparticles. The microstructure and thermoelectric properties of the PbTe-Bi_2Te_3 alloy samples were investigated. The convergent beam electron diffraction (CBED) method and energy dispersive

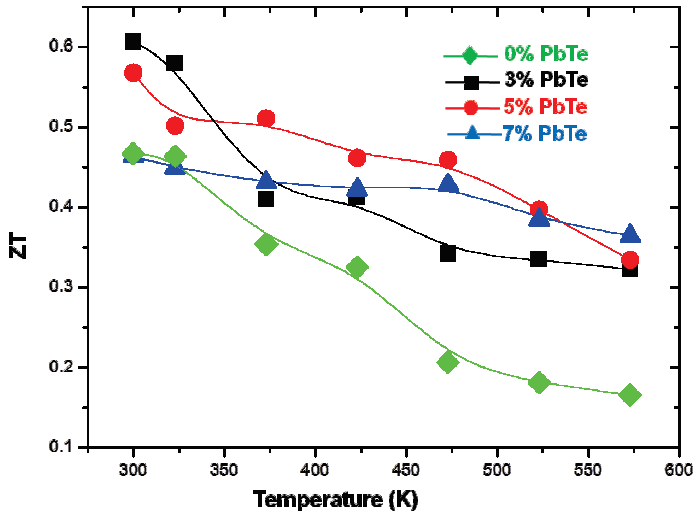

FIG. 6: Temperature dependence of the dimensionless figure of merit for the 0, 3, 5, and 7 wt% PbTe samples.

spectrometer (EDS) analysis using TEM of the PbTe-Bi_2Te_3 alloys reveals three types of phases, a Bi_2Te_3 phase, a $Pb_xBi_{2-x}Te_3$ solid solution, and a $PbBi_2Te_4$ phase depending on the PbTe concentration. The $Pb_xBi_{2-x}Te_3$ solid solution in the Bi_2Te_3 matrix only scatters in phonons, thereby reducing the thermal conductivity. On the other hand, the $PbBi_2Te_4$ phase in the Bi_2Te_3 matrix scatters not only phonons but also electrons. As a result, the maximum ZT values of 0.6 are obtained for the $(PbTe)_3$-$(Bi_2Te_3)_{97}$ alloy at room temperature. It is clear that the reduction in the thermal conductivity plays a key role in the enhancement of the ZT.

Acknowledgments

This work was supported by the Basic Science Research Program through the National Research Foundation of Korea (20110003767), National Research Foundation of Korea Grant funded by the Korean Government (20120000651), Nano Material Technology Development Program through the National Research Foundation of Korea (NRF) funded by the Ministry of Education, Science and Technology (20110030147), and the 'Center for Nanostructured Materials Technology' under the '21st Century Frontier R&D Programs' of the Ministry of Education, Science and Technology, Korea (2011K000197).

References

[1] L. E. Bell, Science **321**, 1457 (2008). doi: 10.1126/science.1158899
[2] M. G. Kanatzidis, Chem. Mater. **22**, 648 (2010). doi: 10.1021/cm902195j
[3] G. J. Snyder and E. S. Toberer, Nat. Mater. **7**, 105 (2008). doi: 10.1038/nmat2090
[4] J. C. Caylor, K. Coonley, J. Stuart, T. Colpitts, and R. Venkatasubramanian, Appl. Phys. Lett. **87**, 023105 (2005). doi: 10.1063/1.1992662
[5] R. Venkatasubramanian, E. Siivola, T. Colpitts, and B. O'Quinn, Nature **413**, 597 (2001). doi: 10.1038/35098012
[6] T. C. Harman, P. J. Taylor, M. P. Walsh, and B. E. LaForge, Science **297**, 2229 (2003).
[7] B. C. Sales, Science **295**, 1248 (2002). doi: 10.1126/science.1069895
[8] M. S. Sander, A. L. Prieto, H. Z. Kou, T. Sands, and A. M. Stacy, Adv. Mater. **14**, 665 (2002).
[9] L. D. Hicks and M. S. Dresselhaus, Phys. Rev. B **47**, 12 (1993).
[10] K. F. Hsu *et al.*, Science **303**, 818 (2004).
[11] G. J. Snyder and E. S. Toberer, Nature Mater. **7**, 105 (2008). doi: 10.1038/nmat2090
[12] J. Sootsman, D. Y. Chung, and M. G. Kanatzidis, Angew. Chem. Int. Ed. **48**, 8616 (2009). doi: 10.1002/anie.200900598
[13] C. J. Vineis, A. Shakouri, A. Majumdar, and M. G. Kanatzidis, Adv. Mater. **22**, 3970 (2010). doi: 10.1002/adma.201000839
[14] L. E. Shelimova, O. G. Karpinskii, V. S. Zemskov *et al.*, Perspekt. Mater. **5**, 23 (2000).
[15] T. Ikeda *et al.*, Chem. Mater. **19**, 763 (2007).
[16] Y. Oosawa, Y. Tateno, M. Mukaida *et al.*, *Proc. XVIII Int. Conf. on Thermoelectrics* (Piscataway, IEEE, 550, 1999).
[17] J.-H. Yim *et al.*, J. Electron. Mater. **40**, 5 (2011).
[18] E. Rogacheva, O. Vodorez, O. Nashchekina, and A. Bondarenko, AIP Conf. Proc. **123**, 1449 (2012). doi: 10.1063/1.4731512
[19] F. J. DiSalvo, Science **285**, 703 (1999). doi: 10.1126/science.285.5428.703
[20] Y. Ma *et al.*, Nano Lett. **8**, 2580 (2008). doi: 10.1021/nl8009928
[21] C. Wood, Rep. Prog. Phys. **51**, 459 (1988). doi: 10.1088/0034-4885/51/4/001
[22] W. McClune, Powder Diffraction File, *JCPDS International Center for Diffraction Data*, Swarthmore, PA.1998.
[23] O. G. Karpinskii, L. E. Shelimova, E. S. Avilov, M. A. Kretova, and V. S. Zemskov, Inorg. Mater. **38**, 17 (2002). doi: 10.1023/A:1013639108297
[24] R. Chami, G. Brun, J.-C. Te'denac, and M. Maurin, Rev. Chim. Miner. **20**, 305 (1983).
[25] L. E. Shelimova *et al.*, Inorg. Mater. **40**, 451 (2004).
[26] L. E. Shelimova *et al.*, Inorg. Mater. **40**, 1264 (2004).
[27] T. B. Zhukowa and A. T. Zaslavskii, Sov. Phys. Crystallogr. **16**, 796 (1971).
[28] R. D. Shannon, Acta Crystallogr. **32A**, 751 (1976).
[29] G. H. Kim, H. S. Kim, and D. H. Kum, Micro. Res. Technol. **33**, 510 (1996). doi: 10.1107/S0567739476001551
[30] W. Kim *et al.*, Phys. Rev. Lett. **96**, 045901 (2006). doi: 10.1103/PhysRevLett.96.045901
[31] J. P. Heremans, C. M. Thrush, and D. T. Morelli, J. Appl. Phys. **98**, 063703 (2005). doi: 10.1063/1.2037209